NANO LETTERS

pubs.acs.org/NanoLett

Letter

Enhanced Electrochemical Methanation of Carbon Dioxide at the Single-Layer Hexagonal Boron Nitride/Cu Interfacial Perimeter

Shaohua Chen,[⊥] Chenyuan Zhu,[⊥] Haoyang Gu, Li Wang, Jiajie Qi, Lixiang Zhong, Zhibin Zhang, Chunlei Yang, Guoshuai Shi, Siwen Zhao, Shuzhou Li, Kaihui Liu,* and Liming Zhang*

Cite This: *Nano Lett.* 2021, 21, 4469−4476

Read Online

ACCESS | Metrics & More | Article Recommendations | Supporting Information

ABSTRACT: The electrochemical conversion of CO_2 to valuable fuels is a plausible solution to meet the soaring need for renewable energy sources. However, the practical application of this process is limited by its poor selectivity due to scaling relations. Here we introduce the rational design of the monolayer hexagonal boron nitride/copper (h-BN/Cu) interface to circumvent scaling relations and improve the electrosynthesis of CH_4. This catalyst possesses a selectivity of >60% toward CH_4 with a production rate of 15 μmol·cm^{-2}·h^{-1} at −1.00 V vs RHE, along with a much smaller decaying production rate than that of pristine Cu. Both experimental and theoretical calculations disclosed that h-BN/Cu interfacial perimeters provide specific chelating sites to immobilize the intermediates, which accelerates the conversion of *CO to *CHO. Our work reports a novel Cu catalyst engineering strategy and demonstrates the prospect of monolayer h-BN contributing to the design of heterostructured CO_2 reduction electrocatalysts for sustainable energy conversion.

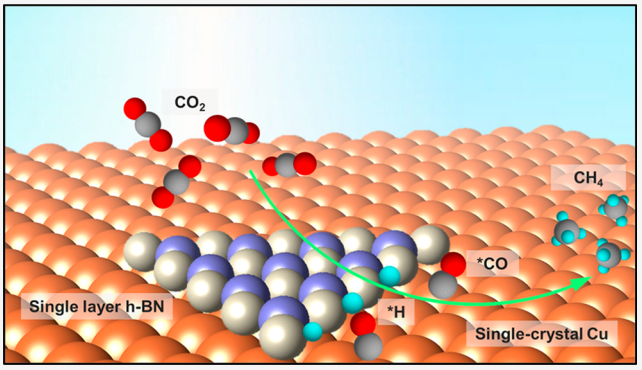

KEYWORDS: *CO_2 reduction, copper, boron nitride, interface, electrochemistry*

INTRODUCTION

CO_2 fixation via electrochemical reduction is an energy-efficient green route to directly convert CO_2 to energy-dense hydrocarbon fuels under a mild condition, which can potentially solve the environmental risks associated with the increasing serious CO_2 emission.[1−3] Despite tremendous efforts over the past decades since the pioneering work of Hori et al. to date, the main challenge for CO_2 reduction (CO_2R) remains the design of a highly active, selective, and stable electrocatalyst.[4,5] Distinguished from the proton reduction, CO_2R exhibits multiple reaction pathways associated with 2−18 electron transfer, leading to a range of value-added carbon fuels [e.g., CO, formate ($HCOO^-$) (both are generated from 2e$^-$ pathways),[6,7] and a series of higher-order products (from multiple >2e$^-$ pathways) such as methane (CH_4), ethylene (C_2H_4), ethanol (C_2H_5OH), and *n*-propanol (*n*-C_3H_7OH), etc.].[8−12] Among various kinds of CO_2R catalysts, copper (Cu) is distinctive in its ability to reduce CO_2 to hydrocarbon products with substantial yields due to its moderate binding energy between metal Cu and intermediates (i.e., CO*).[13−15] However, significant hurdles regarding the poor selectivity of Cu heavily impede electrochemical CO_2R to become a viable and practical option for storing renewable electricity.[16,17]

The preferred reaction pathways of CO_2R on Cu strongly correlate with the interfacial structure.[18−20] For instance, the activation energies of some key steps in CO_2R, such as *CHO formation and *CO dimerization, etc., were recognized as being heavily dependent on the surface facets and morphologies.[21−24] The Cu^+ species on the electrode surface was also proposed to be able to promote the selectivity toward C_{2+} products.[25,26] To improve the selectivity toward hydrocarbons, various strategies of modifying Cu for higher CO_2R performance, such as the control of size,[27,28] surface morphologies,[29,30] chemical states,[26,31] and grain boundaries,[32] have been proposed and have yielded encouraging results.[33] Among the hydrocarbon products in CO_2R, CH_4 is particularly important as a widely used chemical fuel, which can utilize the existing infrastructure for natural gas storage, distribution, and consumption.[34] However, only a few controllable ways to improve the CO_2 to CH_4 conversion selectivity have been reported,[35,36] and more strategies still urgently need to be

Received: March 29, 2021
Revised: May 8, 2021
Published: May 12, 2021

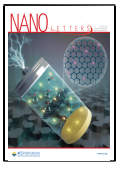

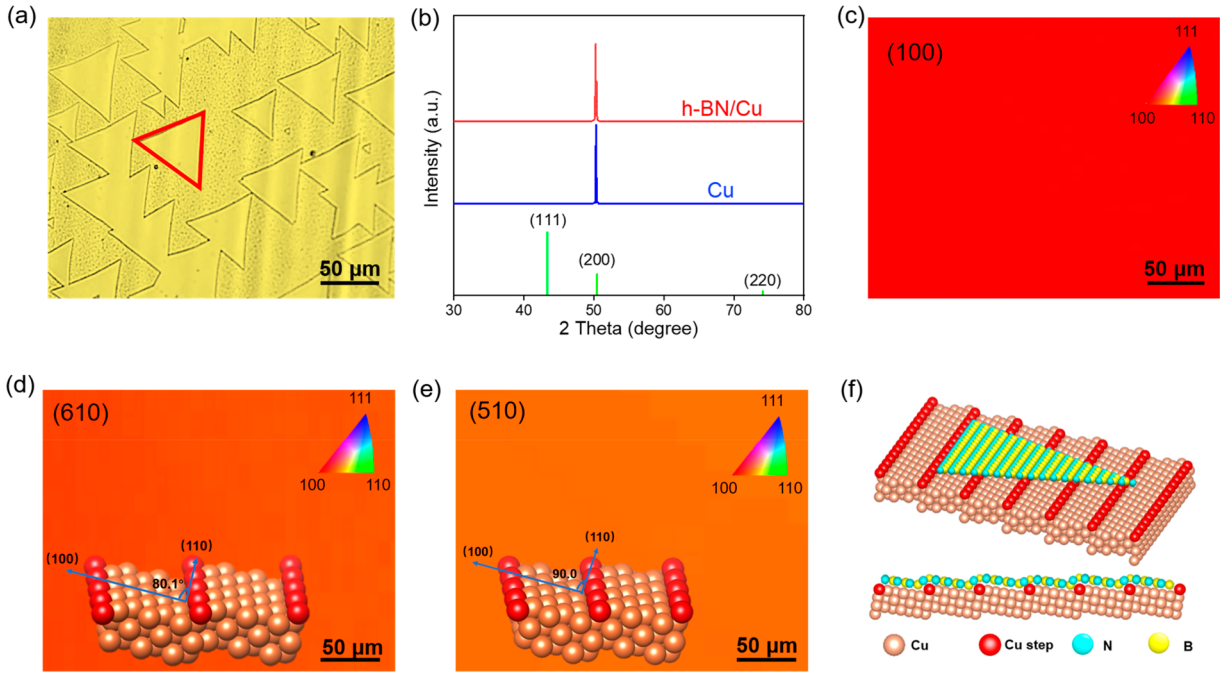

Figure 1. Characterization of monolayer h-BN on single-crystal Cu. (a) Optical graph of h-BN/Cu foil. The red triangular area shows a single h-BN domain on the Cu foil. (b) XRD patterns of Cu substrates with and without h-BN coverage. Green vertical sticks at 43.30, 50.43, and 74.13° are in accordance with the (111), (200), and (220) facets of the fcc Cu (PDF no. 99-0034), respectively. (c–e) Large-scale EBSD mapping of an as-prepared Cu(100) foil (c) and Cu foils after an annealing treatment with (d) and without (e) monolayer h-BN growth, which shows that the surface orientation of Cu(100) has been reconstructed to Cu(610) and Cu(510), respectively. The insets in (d) and (e) show the side views of the atomic schematic illustrations of Cu(610) and Cu(510), respectively. (f) Cartoon figures (both top and side views) highlighting the unidirectional growth of h-BN domains on the single-crystal Cu(610) surface.

developed. In general, the production of CH_4 relies on the following half reaction[37]

$$CO_2 + 8H^+ + 8e^- \rightarrow CH_4 + 2H_2O$$

which involves eight-electron transfer steps that can easily bifurcate to form a variety of fuels, producing a mixture of CH_4, C_2H_4, CO, HCOOH, and H_2 (from the competing proton reduction) due to the well-known scaling relation.[21,38] Therefore, we sought to add a further degree of freedom in catalyst design that would increase the reaction rate of the CH_4 pathway without strongly[39] modulating the others, with the goal of circumventing the scaling relations.[22,40]

Atomic layered hexagonal boron nitride (h-BN) is a two-dimensional (2D) star material with a graphene-like layered structure, where the carbon atoms are substituted by the boron and nitrogen atoms alternatively. h-BN has promising applications in electronic packaging and high-power devices, owing to its high thermal conductivity, excellent thermal/chemical stability, and ultrawide band gap.[41,42] As an insulator with strong stability, h-BN is also widely used as a nanofiller in the field of metal anticorrosion.[42−44] Although various progress has been made in the chemical synthesis and physical properties of h-BN, its catalytic characteristics are rarely explored.[45] In this work, we focus on the interface between Cu and h-BN by uniformly growing a monolayer of h-BN on the Cu surface to trigger the selective production of CH_4 from CO_2R. The obtained interface of h-BN/Cu exhibits superior activity toward CO_2R over proton reduction. More importantly, the selectivity of CH_4 is dramatically increased from ∼14% on pure Cu to >60% on the h-BN/Cu interface. Both experimental and density functional theoretical (DFT) calculations disclosed that the h-BN/Cu perimeter provides specific chelating sites to stably immobilize the reaction intermediates, and this unique catalytic coupling synergistically contributes to this distinguished CH_4 production. Our findings demonstrate an important discovery in engineering the interface of Cu catalysts, and lend credence to the prospect of single-layer h-BN contributing to the design of hetero-structured CO_2R electrocatalysts for sustainable energy conversion.

RESULTS AND DISCUSSION

The h-BN/Cu heterostructure was prepared following our recently developed strategy with modified conditions.[41] Typically, 5 cm × 5 cm single-crystal Cu foils having an exposed Cu(100) facet were prepared by annealing industrial polycrystalline Cu foils using a designed high-temperature pretreatment. When Cu(100) was used as the substrate, 2D h-BN was subsequently synthesized via a low-pressure chemical vapor deposition (CVD) strategy with ammonia borane (H_3B-NH_3) as the feedstock (details in Supporting Information). As shown in the optical graph (Figure 1a), large-area triangular h-BN domains with a side length of ∼50 μm cover the Cu substrate evenly. Atomic force microscopy (AFM) confirmed the successful formation of h-BN with a thickness of <1 nm (Supporting Information Figure S1), corresponding to the single-layer thickness. In particular, the optical graph revealed that the h-BN domains grown on the Cu surface were all triangular, with their domains aligned unidirectionally on Cu, indicating that all domains had the same crystalline orientation (Supporting Information Figure S2).

We further monitored the crystal orientation of the Cu substrate using X-ray diffraction (XRD). The sharp Cu(200) peak in the 2θ scan with and without h-BN coverage indicates

https://doi.org/10.1021/acs.nanolett.1c01258
Nano Lett. 2021, 21, 4469−4476

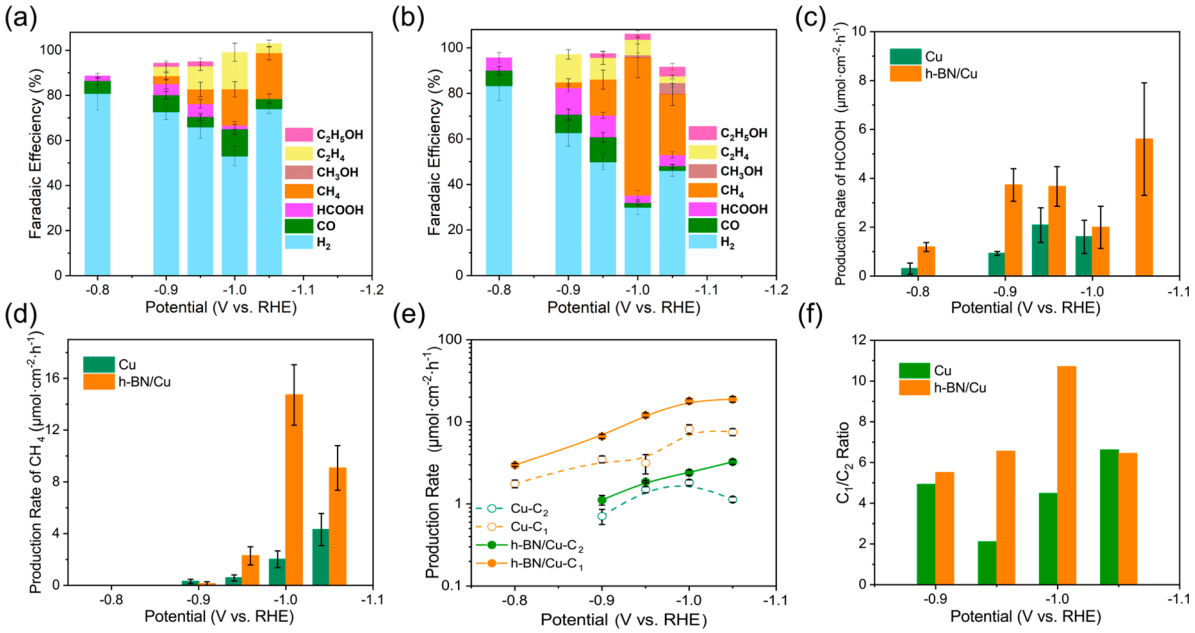

Figure 2. CO_2R electrocatalysis comparison between h-BN/Cu and Cu. (a, b) Comparison of the CO_2R product distributions on Cu (a) and h-BN/Cu (b). (c, d) Comparison of the production rates of HCOOH (c) and CH_4 (d) in the potential range from −0.80 to −1.05 V vs RHE on Cu and h-BN/Cu, respectively. (e) Summary of C_1 and C_2 conversion rates on h-BN/Cu and Cu. (f) Ratios of C_1/C_2 products under different applied potentials. All of the electrochemical performances were tested in a 0.1 M $KHCO_3$ aqueous solution under 1 atm of CO_2 in a two-compartment H-cell, and the error bars represent the standard deviation of triplicate measurements.

that the growth of h-BN will not alter the orientation of single-crystal Cu substrates in the bulk (Figure 1b). On the contrary, the growth of h-BN under high temperature induced Cu surface reconstruction, from Cu(100) to (610) on the top surface, as evidenced by the uniform color contrast of electron back-scattered diffraction (EBSD) mapping (Figure 1c,d). We also tested the surface reconstruction of the control sample, which was treated at the same temperature without the H_3B-NH_3 precursor feed, and observed that the surface of Cu was reconstructed from Cu(100) to Cu(510) instead (Figure 1e). Both Cu(610) and Cu(510) facets, denoted as Cu(S)-[1_1(110)+5_5(100)] and Cu(S)-[1_1(110)+4_4(100)], respectively, can be visualized as kinked surfaces with narrow (100) terraces and a high density of (110) steps. The angles between the terrace and step of Cu(610) and Cu(510) are 80.1 and 90.0°, respectively (insets of Figure 1d,e). Thus, given the strong coupling between Cu(110) edges and h-BN, we can deduce that the unidirectional alignment of h-BN domains was caused by the step-edge-mediated nucleation due to the presence of parallel step edges (from the uniform surface tilt angle) on the high-index single-crystal Cu facets. The resulting h-BN/Cu heterostructure is schematically illustrated in Figure 1f.

Next, the electrocatalytic CO_2R performance of the h-BN/Cu heterostructure was evaluated using a bare Cu substrate treated at the same temperature without h-BN growth as a control sample. Each sample was tested at multiple potentials, and the gas and liquid products were quantified using gas chromatography (GC) and nuclear magnetic resonance (NMR) spectroscopy, respectively. (See the details in Supporting Information Figures S3 and S4.) The linear sweep voltammetry (LSV), the product distribution, and the partial current density on both Cu and h-BN/Cu were plotted as a function of applied potential, as summarized in Figure 2a,b and Supporting Information Figures S5 and S6. It can be observed that the bare Cu catalyst exhibited a similar product distribution to that of metallic Cu reported previously,[46] namely, generating more hydrocarbon products, such as CH_4 and C_2H_4, than oxygenates. An improved electrochemical CO_2R performance on h-BN/Cu is evidenced by both significantly enhanced total Faradaic efficiencies (FEs) and production rates. In the potential window examined from −0.80 to −1.05 V vs RHE, <46% of FEs are attributed to CO_2R on pure Cu, and a large current has been consumed for proton reduction. In contrast, the introduction of the h-BN/Cu interface promotes the reduction of CO_2 across a wide potential window (e.g., the overall FEs toward CO_2R (non-hydrogen products) increases from 21, 29, 46, and 28% to 34, 52, 75, and 45%, respectively, in the range of −0.90 to −1.05 V vs RHE, with a −50 mV step increment. The large difference in product distributions between Cu and h-BN/Cu is mostly contributed by the improved generation of higher-order C_1 products. Specifically, at −1.00 V vs RHE, the FE of CH_4 achieves a fairly high value of >60% on the interface of h-BN/Cu, showing a 4-fold enhancement compared to that of bare Cu at the same potential and being among the best performances in various Cu-based electrocatalysts for CH_4-selective production (Supporting Information Table S1). Beyond CH_4, what is surprising is the detection of CH_3OH, which, although the amount is not significant (FE ≈ 5%), is rarely reported for Cu-based catalysts in electrochemical CO_2R.

To identify the specific fuel production with and without h-BN coverage clearly, we grouped CO_2R products as C_1 products (e.g., CO, HCOOH, CH_4, and CH_3OH) and C_2 products, including C_2H_4 and C_2H_5OH. We calculated the generation rates of both C_1 and C_2 products from the partial current densities on h-BN/Cu and Cu, respectively (Supporting Information Figure S7). Among C_1 products, HCOOH is considered to be a terminal $2e^-$ pathway formed through a

https://doi.org/10.1021/acs.nanolett.1c01258
Nano Lett. 2021, 21, 4469−4476

different mechanism apart from CO, CH_4, and CH_3OH.[18] As shown in Figure 2c, the conversion rate of CO_2 to HCOOH is higher on h-BN/Cu across the full potential window from −0.80 to −1.05 V vs RHE and achieves the maximum value at −1.05 V vs RHE, under which the HCOOH production is even unobservable on pure Cu. As mentioned already, the increase in the CH_4 production rate is significantly improved by covering Cu with h-BN (Figure 2d), with a conversion rate sharply increased by more than 7-fold at −1.00 V vs RHE, from 2 to 15 $\mu mol \cdot cm^{-2} \cdot h^{-1}$. It is also notable that the production of CH_3OH was observed on h-BN/Cu at −1.00 V vs RHE (Supporting Information Figure S8). These results indicate that the conversion of CO_2 to C_1 products is highly promoted at the interface of h-BN/Cu. On the contrary, the presence of the h-BN/Cu interface leads to a suppression of CO production [e.g., the generation of CO decreased by more than 2 times on h-BN/Cu at −1.0 V vs RHE (Supporting Information Figure S9)], indicative of the competitive reaction pathways between HCOOH and CO and the further consumption of CO* intermediates for higher-order products. The higher production rate of CO on Cu can be ascribed to the weaker binding energy between metal Cu and CO* intermediates, while the stronger binding energy between h-BN/Cu and CO* would promote the formation of higher-order C_1 products. It is worth noting that on h-BN/Cu the increase in C_2 production is inconspicuous as compared to the increase in C_1 (Supporting Information Figure S10). This means that CO*−CO* coupling, which generally depends on the concentration of CO* on the interface, would not be largely influenced by the h-BN/Cu interface. As shown in Figure 2e, we next summarized the conversion rate of C_1 and C_2 products at different potentials on h-BN/Cu and Cu and observed that the introduction of h-BN significantly increases the conversion of CO_2 to C_1 products by almost 1 order of magnitude. In particular, the conversion ratio of C_1/C_2 that is achieved is larger than 10 at −1.00 V vs RHE (Figure 2f), and this ratio is in the top rank of the most reported Cu-based CO_2R electrocatalysts (Supporting Information Table 2). Tafel slopes were estimated by plotting the logarithm of the CH_4 partial current density with applied potential, indicating that h-BN/Cu has more rapid kinetics toward CH_4 production (Supporting Information Figure S11).

To investigate the influence of h-BN on Cu, the possible contribution from the different facets of Cu [(510) for bare Cu and (610) for h-BN/Cu] was first excluded by peeling off the h-BN layer through electrochemical polishing and testing the CO_2R performance of the obtained bare Cu(610). The peeling-off process will not change the surface orientation of Cu (Supporting Information Figure S12). The FEs of both C_1 and C_2 products are close to those of bare Cu(510) (having differences of within 5%), indicating that the crystal facet is not the main cause of the accelerated methanation process (Supporting Information Figure S13).

To further understand the superiority of h-BN/Cu heterostructure for C_1 production, we investigated the influence of h-BN coverage on the product distribution. The coverage of h-BN domains can be well controlled by the growth time, and the domains are gradually stitched into an intact piece of film seamlessly as time increases. The coverage and corresponding boundary length of the h-BN film on the Cu substrate were statistically calculated by optical graphs via mathematical means to depict all of the boundary lengths of the h-BN film within the selected area. (See more details in the Supporting Information.) Here we chose five h-BN/Cu samples with 31 ± 6, 43 ± 5, 64 ± 9, 86 ± 8, and 98 ± 2% h-BN coverage (Figure 3a). The corresponding relationship

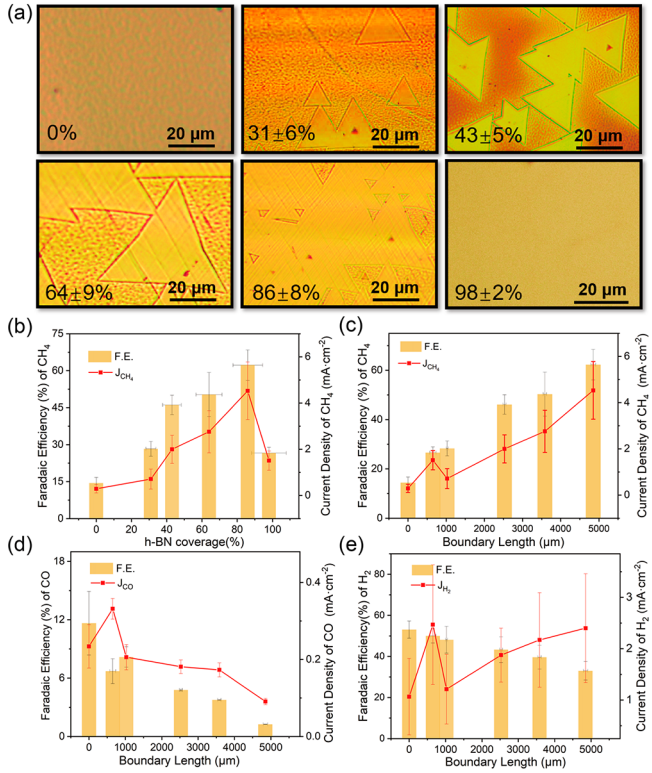

Figure 3. Product quantification on h-BN/Cu foils having different h-BN coverages. (a) Optical graphs of as-prepared h-BN/Cu samples having different h-BN coverages. (b, c) Correlation between FE (%) as well as partial current density of CH_4 with h-BN coverage (b) and the h-BN/Cu interfacial perimeter (c) at −1.00 V vs RHE. (d, e) The FEs and partial current density of CO (d) and H_2 (e) on the h-BN/Cu foil with the h-BN/Cu interfacial perimeter at −1.00 V vs RHE, respectively. All of the electrochemical performances were tested in a 0.1 M $KHCO_3$ aqueous solution under 1 atm of CO_2 in a two-compartment H-cell, and the error bars represent the standard deviation of triplicate measurements.

between different coverages and lengths of the h-BN/Cu interfacial perimeter was also plotted (Supporting Information Figure S14). We first demonstrated the relationship between CH_4 selectivity and the coverage of the h-BN film (Figure 3b). After h-BN introduction, both the FE and partial current density of CH_4 exhibit an obviously increasing tendency until the surface coverage of h-BN reaches 86%. However, when the coverage of h-BN achieves 98%, which means that the surface of Cu is nearly coated with the h-BN film, the selectivity of CH_4 decreased drastically to 28%. This result indicates that the coverage of an intact h-BN film is not the crucial cause of the preference for CH_4 production. Instead, we observed an interesting rough linear dependence between the h-BN/Cu interfacial perimeter (boundary length) and the FE of CH_4. As shown in Figure 3c, the FE of CH_4 linearly increases with the increase in the h-BN/Cu boundary length, with a slope of 1.1%/μm. For the samples with 98% h-BN coverage, the boundary length of h-BN/Cu is sharply decreased with the merging of the h-BN film, the selectivity of CH_4 was accordingly decreased. These results demonstrate a slightly improved turnover frequency (TOF) of CH_4 at a larger

https://doi.org/10.1021/acs.nanolett.1c01258
Nano Lett. 2021, 21, 4469−4476

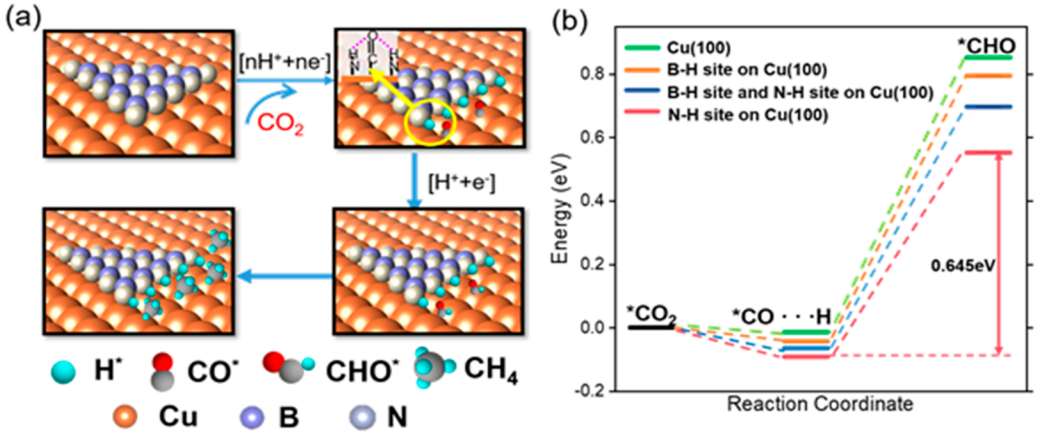

Figure 4. DFT calculations of the CO_2 conversion to CH_4 at the h-BN/Cu interface. (a) Schematic illustrations of the intermediates on the h-BN/Cu boundary with N-atom termination. (b) Calculated free-energy diagrams comparing the further reduction of CO* to CHO*, an important step for CH_4 production, on bare Cu and three h-BN/Cu interfaces having different edge terminations.

coverage condition (Supporting Information Figure S15) and indicate that the h-BN/Cu interfacial perimeter plays a crucial role in the methanation process. It is also notable to observe that, in comparison with CH_4, CO production has a reverse correlation with the h-BN boundary length, which further proves that most of the adsorbed CO* intermediates are consumed to generate higher-order C_1 products (Figure 3d). Although the partial current density of H_2 exhibits a growing trend along with the boundary length extended, which indicates the activation of H* intermediates, the FE of H_2 showed a decreasing tendency with the increase in h-BN/Cu boundaries (Figure 3e). These results reveal the importance of the h-BN/Cu interfacial perimeter in improving the activity toward CO_2 to CH_4 conversion.

To determine whether the morphology and surface composition of the h-BN/Cu electrode changed during CO_2R, h-BN/Cu samples were characterized after electrocatalysis by atomic force microscopy (AFM). AFM images show that after 2 h of electrolysis at −1.00 V vs RHE, most of the edge sites of the h-BN triangular flake (as pointed out by the blue arrow) remain unaffected (AFM images are shown in Supporting Information Figure S16a), and the FE of CH_4 is maintained at >50% in this period. With the reaction time increasing to 4 h, we observed a slightly decreased CH_4 production rate (Supporting Information Figure S16c), which is attributed to the partially blocked edges of h-BN by the growing Cu dendrites (Supporting Information Figure S16b). However, in comparison to bare Cu, the decreasing rate of CH_4 production obviously slowed down, with the production rate decaying only by 9% in 4 h, which is much smaller than that of bare Cu. These results suggest the crucial protective role of the h-BN atomic layer.

DFT calculations were carried out to investigate whether the h-BN/Cu interface can help to adsorb C_1 intermediates.[47] Generally, the reduction of CO_2 to CH_4 starts with the hydrogenation of an adsorbed $*CO_2$ to form *COOH. Following further reaction and OH desorption, CO* is left on the surface and the third protonation process occurs to form *CHO,[48] which is usually considered to be a rate-limiting step. This suggests that narrowing the energy barrier of *CHO formation can greatly promote CH_4 production. The Cu(100) facet is chosen since other facets are not the main cause of the accelerated methanation process. Three different kinds of active sites (H-terminated armchair h-BN, H-terminated zigzag h-BN having boron atoms exposed on the edge, and H-terminated zigzag h-BN having nitrogen atoms exposed on the edge) located on Cu(100) were listed as candidates for modeling the interaction between h-BN/Cu boundary and adsorbed CO* and CHO*. Figure 4a illustrates the process of *CO conversion to *CHO. In an aqueous solution, boron and nitrogen atoms at both the armchair and zigzag h-BN/Cu boundaries prefer to adsorb H atoms in order to remain stable, and the three different obtained edges listed above can be denoted as BN−H, B−H, and N−H, respectively. In regard to the generation of *CHO, N−H sites can form two hydrogen bonds with adsorbed CO* (N−H···O−C) as depicted in Figure 4a, and the corresponding energy barrier for this process is calculated to be 0.645 eV, which is much smaller in comparison to the other two h-BN/Cu boundaries. (Figure 4b and Supporting Information Figure S17). More importantly, all three edges demonstrate a smaller energy barrier than that on bare Cu, and this result suggests that the synergistic effect of interactions between Cu and h-BN presents a novel strategy for designing highly selective CO_2R electrocatalysts toward $>2e^-$ C_1 products, such as CH_4 in this work.

CONCLUSIONS

We demonstrated a novel heterogeneous h-BN/Cu interface to circumvent the scaling relations in electrochemical CO_2R. Upon decorating a single layer of h-BN, the current density of the CO_2R was thus increased at the h-BN/Cu interface. More importantly, the higher-order C_1 products have become the major products. At −1.00 V vs RHE, for example, the FE of CH_4 increased from ca. 15% (on pristine Cu) to >60% (on h-BN/Cu), with the production rate enhanced by 7-fold. Such a great change is not a result of the crystal orientation change of the Cu surface but is rather a synergistic catalytic effect of the h-BN/Cu interface. Experimental results have shown that by increasing the interfacial perimeter of h-BN/Cu, both the CH_4 selectivity and partial current density are promoted. DFT calculations further reveal that the h-BN/Cu perimeter provides specific chelating sites to stably immobilize the CHO* intermediates, with this unique catalytic coupling synergistically contributing to this distinguished CH_4 production. Our findings open up a promising avenue to tuning the catalytic activity, selectivity, and stability of Cu toward CO_2R, not through the structure engineering of Cu itself but through

https://doi.org/10.1021/acs.nanolett.1c01258
Nano Lett. 2021, 21, 4469−4476

marrying Cu with another single-layer component and creating synergy.

■ ASSOCIATED CONTENT

Supporting Information

The Supporting Information is available free of charge at https://pubs.acs.org/doi/10.1021/acs.nanolett.1c01258.

Detailed methods and characterization of h-BN/Cu and their electrochemical CO_2 reduction properties (PDF)

■ AUTHOR INFORMATION

Corresponding Authors

Kaihui Liu − *State Key Laboratory for Mesoscopic Physics, Frontiers Science Center for Nano-optoelectronics, School of Physics, Peking University, Beijing 100871, China;* orcid.org/0000-0002-8781-2495; Email: khliu@pku.edu.cn

Liming Zhang − *Department of Chemistry and Shanghai Key Laboratory of Molecular Catalysis and Innovative Materials, Fudan University, Shanghai 200438, China;* orcid.org/0000-0001-6795-3381; Email: zhanglm@fudan.edu.cn

Authors

Shaohua Chen − *Department of Chemistry and Shanghai Key Laboratory of Molecular Catalysis and Innovative Materials, Fudan University, Shanghai 200438, China*

Chenyuan Zhu − *Department of Chemistry and Shanghai Key Laboratory of Molecular Catalysis and Innovative Materials, Fudan University, Shanghai 200438, China*

Haoyang Gu − *Department of Chemistry and Shanghai Key Laboratory of Molecular Catalysis and Innovative Materials, Fudan University, Shanghai 200438, China*

Li Wang − *Beijing National Laboratory for Condensed Matter Physics, Institute of Physics, Chinese Academy of Sciences, Beijing, China*

Jiajie Qi − *State Key Laboratory for Mesoscopic Physics, Frontiers Science Center for Nano-optoelectronics, School of Physics, Peking University, Beijing 100871, China;* orcid.org/0000-0003-3140-7842

Lixiang Zhong − *School of Materials Science and Engineering, Nanyang Technological University, Singapore 639798, Singapore;* orcid.org/0000-0002-8975-9392

Zhibin Zhang − *State Key Laboratory for Mesoscopic Physics, Frontiers Science Center for Nano-optoelectronics, School of Physics, Peking University, Beijing 100871, China*

Chunlei Yang − *Department of Chemistry and Shanghai Key Laboratory of Molecular Catalysis and Innovative Materials, Fudan University, Shanghai 200438, China*

Guoshuai Shi − *Department of Chemistry and Shanghai Key Laboratory of Molecular Catalysis and Innovative Materials, Fudan University, Shanghai 200438, China*

Siwen Zhao − *Department of Chemistry and Shanghai Key Laboratory of Molecular Catalysis and Innovative Materials, Fudan University, Shanghai 200438, China*

Shuzhou Li − *School of Materials Science and Engineering, Nanyang Technological University, Singapore 639798, Singapore;* orcid.org/0000-0002-2159-2602

Complete contact information is available at: https://pubs.acs.org/10.1021/acs.nanolett.1c01258

Author Contributions

L.Z. designed and conceived the experiment. S.C., C.Z., H.G., G.S., and S.Z. fabricated and characterized the electrodes and performed the electrochemical characterization and data analysis. L.W., J.Q., Z.Z., and K.L. carried out the synthesis of the h-BN/Cu electrode and performed EBSD and AFM characterizations. L.Z. and S.L. worked on the DFT calculations. All authors discussed the results and participated in writing the manuscript.

Author Contributions

$^{\perp}$S.C. and C.Z. contributed equally to this work.

Notes

The authors declare no competing financial interest.

■ ACKNOWLEDGMENTS

This research was supported by the National Natural Science Foundation of China (grants 21872039, 22072030, and 52025023) and the Science and Technology Commission of Shanghai Municipality (grants 18JC1411700 and 19DZ2270100).

■ REFERENCES

(1) Aresta, M.; Dibenedetto, A.; Angelini, A. Catalysis for the Valorization of Exhaust Carbon: from CO_2 to Chemicals, Materials, and Fuels. Technological Use of CO_2. *Chem. Rev.* **2014**, *114* (3), 1709−1742.

(2) Tang, F.; Wang, L.; Liu, Y. N. Biomass-derived N-doped porous carbon: an efficient metal-free catalyst for methylation of amines with CO_2. *Green Chem.* **2019**, *21* (23), 6252−6257.

(3) Birdja, Y. Y.; Pérez-Gallent, E.; Figueiredo, M. C.; Göttle, A. J.; Calle-Vallejo, F.; Koper, M. T. M. Advances and challenges in understanding the electrocatalytic conversion of carbon dioxide to fuels. *Nat. Energy* **2019**, *4* (9), 732−745.

(4) Hori, Y.; Murata, A.; Takahashi, R. Formation of hydrocarbons in the electrochemical reduction of carbon dioxide at a copper electrode in aqueous solution. *J. Chem. Soc., Faraday Trans. 1* **1989**, *85* (8), 2309−2326.

(5) Hori, Y.; Takahashi, I.; Koga, O.; Hoshi, N. Electrochemical reduction of carbon dioxide at various series of copper single crystal electrodes. *J. Mol. Catal. A: Chem.* **2003**, *199* (1−2), 39−47.

(6) Liu, S.; Xiao, J.; Lu, X. F.; Wang, J.; Wang, X.; Lou, X. W. D. Efficient Electrochemical Reduction of CO_2 to HCOOH over Sub-2 nm SnO_2 Quantum Wires with Exposed Grain Boundaries. *Angew. Chem., Int. Ed.* **2019**, *58* (25), 8499−8503.

(7) Nellaiappan, S.; Katiyar, N. K.; Kumar, R.; Parui, A.; Malviya, K. D.; Pradeep, K. G.; Singh, A. K.; Sharma, S.; Tiwary, C. S.; Biswas, K. High-Entropy Alloys as Catalysts for the CO_2 and CO Reduction Reactions: Experimental Realization. *ACS Catal.* **2020**, *10* (6), 3658−3663.

(8) Kuhl, K. P.; Cave, E. R.; Abram, D. N.; Jaramillo, T. F. New insights into the electrochemical reduction of carbon dioxide on metallic copper surfaces. *Energy Environ. Sci.* **2012**, *5* (5), 7050−7059.

(9) Gao, D.; Arán-Ais, R. M.; Jeon, H. S.; Roldan Cuenya, B. Rational catalyst and electrolyte design for CO_2 electroreduction towards multicarbon products. *Nat. Catal.* **2019**, *2* (3), 198−210.

(10) Li, Z.; Yang, Y.; Yin, Z.; Wei, X.; Peng, H.; Lyu, K.; Wei, F.; Xiao, L.; Wang, G.; Abruña, H. D.; Lu, J.; Zhuang, L. Interface-Enhanced Catalytic Selectivity on the C_2 Products of CO_2 Electroreduction. *ACS Catal.* **2021**, *11* (5), 2473−2482.

(11) Ma, S.; Sadakiyo, M.; Heima, M.; Luo, R.; Haasch, R. T.; Gold, J. I.; Yamauchi, M.; Kenis, P. J. Electroreduction of Carbon Dioxide to Hydrocarbons Using Bimetallic Cu-Pd Catalysts with Different Mixing Patterns. *J. Am. Chem. Soc.* **2017**, *139* (1), 47−50.

(12) Pang, Y.; Li, J.; Wang, Z.; Tan, C. S.; Hsieh, P. L.; Zhuang, T. T.; Liang, Z. Q.; Zou, C.; Wang, X.; De Luna, P.; Edwards, J. P.; Xu, Y.; Li, F.; Dinh, C. T.; Zhong, M.; Lou, Y.; Wu, D.; Chen, L. J.;

Sargent, E. H.; Sinton, D. Efficient electrocatalytic conversion of carbon monoxide to propanol using fragmented copper. *Nat. Catal.* **2019**, *2* (3), 251−258.
(13) Nitopi, S.; Bertheussen, E.; Scott, S. B.; Liu, X.; Engstfeld, A. K.; Horch, S.; Seger, B.; Stephens, I. E. L.; Chan, K.; Hahn, C.; Nørskov, J. K.; Jaramillo, T. F.; Chorkendorff, I. Progress and Perspectives of Electrochemical CO_2 Reduction on Copper in Aqueous Electrolyte. *Chem. Rev.* **2019**, *119* (12), 7610−7672.
(14) Bagger, A.; Ju, W.; Varela, A. S.; Strasser, P.; Rossmeisl, J. Electrochemical CO_2 Reduction: A Classification Problem. *ChemPhysChem* **2017**, *18* (22), 3266−3273.
(15) Wu, Y.; Jiang, Z.; Lu, X.; Liang, Y.; Wang, H. Domino electroreduction of CO_2 to methanol on a molecular catalyst. *Nature* **2019**, *575* (7784), 639−642.
(16) Appel, A. M.; Bercaw, J. E.; Bocarsly, A. B.; Dobbek, H.; DuBois, D. L.; Dupuis, M.; Ferry, J. G.; Fujita, E.; Hille, R.; Kenis, P. J. A.; Kerfeld, C. A.; Morris, R. H.; Peden, C. H. F.; Portis, A. R.; Ragsdale, S. W.; Rauchfuss, T. B.; Reek, J. N. H.; Seefeldt, L. C.; Thauer, R. K.; Waldrop, G. L. Frontiers, Opportunities, and Challenges in Biochemical and Chemical Catalysis of CO_2 Fixation. *Chem. Rev.* **2013**, *113* (8), 6621−6658.
(17) Spurgeon, J. M.; Kumar, B. A comparative technoeconomic analysis of pathways for commercial electrochemical CO_2 reduction to liquid products. *Energy Environ. Sci.* **2018**, *11* (6), 1536−1551.
(18) Rendón-Calle, A.; Builes, S.; Calle-Vallejo, F. A brief review of the computational modeling of CO_2 electroreduction on Cu electrodes. *Curr. Opin. Electrochem.* **2018**, *9*, 158−165.
(19) Lu, Q.; Jiao, F. Electrochemical CO_2 reduction: Electrocatalyst, reaction mechanism, and process engineering. *Nano Energy* **2016**, *29*, 439−456.
(20) Wang, J.; Cheng, C.; Huang, B.; Cao, J.; Li, L.; Shao, Q.; Zhang, L.; Huang, X. Grain-Boundary-Engineered La_2CuO_4 Perovskite Nanobamboos for Efficient CO_2 Reduction Reaction. *Nano Lett.* **2021**, *21* (2), 980−987.
(21) Peterson, A. A.; Nørskov, J. K. Activity Descriptors for CO_2 Electroreduction to Methane on Transition-Metal Catalysts. *J. Phys. Chem. Lett.* **2012**, *3* (2), 251−258.
(22) Wei, X.; Yin, Z.; Lyu, K.; Li, Z.; Gong, J.; Wang, G.; Xiao, L.; Lu, J.; Zhuang, L. Highly Selective Reduction of CO_2 to C_{2+} Hydrocarbons at Copper/Polyaniline Interfaces. *ACS Catal.* **2020**, *10* (7), 4103−4111.
(23) Zhao, S.; Tang, Z.; Guo, S.; Han, M.; Zhu, C.; Zhou, Y.; Bai, L.; Gao, J.; Huang, H.; Li, Y.; Liu, Y.; Kang, Z. Enhanced Activity for CO_2 Electroreduction on a Highly Active and Stable Ternary Au-CDots-C_3N_4 Electrocatalyst. *ACS Catal.* **2018**, *8* (1), 188−197.
(24) Vasileff, A.; Xu, C.; Jiao, Y.; Zheng, Y.; Qiao, S. Z. Surface and Interface Engineering in Copper-Based Bimetallic Materials for Selective CO_2 Electroreduction. *Chem.* **2018**, *4* (8), 1809−1831.
(25) Kim, D.; Kley, C. S.; Li, Y.; Yang, P. Copper nanoparticle ensembles for selective electroreduction of CO_2 to C_2-C_3 products products. *Proc. Natl. Acad. Sci. U. S. A.* **2017**, *114* (40), 10560.
(26) Cheng, D.; Zhao, Z. J.; Zhang, G.; Yang, P.; Li, L.; Gao, H.; Liu, S.; Chang, X.; Chen, S.; Wang, T.; Ozin, G. A.; Liu, Z.; Gong, J. The nature of active sites for carbon dioxide electroreduction over oxide-derived copper catalysts. *Nat. Commun.* **2021**, *12* (1), 395.
(27) Liu, J.; Guo, C.; Vasileff, A.; Qiao, S. Nanostructured 2D Materials: Prospective Catalysts for Electrochemical CO_2 Reduction. *Small Methods* **2017**, *1* (1−2), 1600006.
(28) Reske, R.; Mistry, H.; Behafarid, F.; Roldan Cuenya, B.; Strasser, P. Particle size effects in the catalytic electroreduction of CO_2 on Cu nanoparticles. *J. Am. Chem. Soc.* **2014**, *136* (19), 6978−86.
(29) Zhu, C.; Zhang, Z.; Zhong, L.; Hsu, C. S.; Xu, X.; Li, Y.; Zhao, S.; Chen, S.; Yu, J.; Chen, S.; Wu, M.; Gao, P.; Li, S.; Chen, H. M.; Liu, K.; Zhang, L. Product-Specific Active Site Motifs of Cu for Electrochemical CO_2 Reduction. *Chem.* **2021**, *7* (2), 406−420.
(30) De Luna, P.; Quintero-Bermudez, R.; Dinh, C. T.; Ross, M. B.; Bushuyev, O. S.; Todorović, P.; Regier, T.; Kelley, S. O.; Yang, P.; Sargent, E. H. Catalyst electro-redeposition controls morphology and oxidation state for selective carbon dioxide reduction. *Nat. Catal.* **2018**, *1* (2), 103−110.
(31) Chou, T.-C.; Chang, C.-C.; Yu, H. L.; Yu, W. Y.; Dong, C. L.; Velasco-Vélez, J. J.; Chuang, C. H.; Chen, L. C.; Lee, J. F.; Chen, J. M.; Wu, H. L. Controlling the Oxidation State of the Cu Electrode and Reaction Intermediates for Electrochemical CO_2 Reduction to Ethylene. *J. Am. Chem. Soc.* **2020**, *142* (6), 2857−2867.
(32) Tang, C.; Shi, J.; Bai, X.; Hu, A.; Xuan, N.; Yue, Y.; Ye, T.; Liu, B.; Li, P.; Zhuang, P.; Shen, J.; Liu, Y.; Sun, Z. CO_2 Reduction on Copper's Twin Boundary. *ACS Catal.* **2020**, *10* (3), 2026−2032.
(33) Lee, M. Y.; Park, K. T.; Lee, W.; Lim, H.; Kwon, Y.; Kang, S. Current achievements and the future direction of electrochemical CO_2 reduction: A short review. *Crit. Rev. Environ. Sci. Technol.* **2020**, *50* (8), 769−815.
(34) MacDonald, G. J. The Future of Methane as an Energy Resource. *Annu. Rev. Energy* **1990**, *15* (1), 53−83.
(35) Handoko, A. D.; Chan, K. W.; Yeo, B. S. -CH_3 Mediated Pathway for the Electroreduction of CO_2 to Ethane and Ethanol on Thick Oxide-Derived Copper Catalysts at Low Overpotentials. *ACS Energy Lett.* **2017**, *2* (9), 2103−2109.
(36) Li, Y.; Cui, F.; Ross, M. B.; Kim, D.; Sun, Y.; Yang, P. Structure-Sensitive CO_2 Electroreduction to Hydrocarbons on Ultrathin 5-fold Twinned Copper Nanowires. *Nano Lett.* **2017**, *17* (2), 1312−1317.
(37) Manthiram, K.; Beberwyck, B. J.; Alivisatos, A. P. Enhanced Electrochemical Methanation of Carbon Dioxide with a Dispersible Nanoscale Copper Catalyst. *J. Am. Chem. Soc.* **2014**, *136* (38), 13319−13325.
(38) Li, Y.; Sun, Q. Recent Advances in Breaking Scaling Relations for Effective Electrochemical Conversion of CO_2. *Adv. Energy Mater.* **2016**, *6* (17), 1600463.
(39) Chen, T. A.; Chuu, C. P.; Tseng, C. C.; Wen, C. K.; Wong, H. P.; Pan, S.; Li, R.; Chao, T. A.; Chueh, W. C.; Zhang, Y.; Fu, Q.; Yakobson, B. I.; Chang, W. H.; Li, L. J. Wafer-scale single-crystal hexagonal boron nitride monolayers on Cu (111). *Nature* **2020**, *579* (7798), 219−223.
(40) Wang, H.; Tzeng, Y. K.; Ji, Y.; Li, Y.; Li, J.; Zheng, X.; Yang, A.; Liu, Y.; Gong, Y.; Cai, L.; Li, Y.; Zhang, X.; Chen, W.; Liu, B.; Lu, H.; Melosh, N. A.; Shen, Z. X.; Chan, K.; Tan, T.; Chu, S.; Cui, Y. Synergistic enhancement of electrocatalytic CO_2 reduction to C_2 oxygenates at nitrogen-doped nanodiamonds/Cu interface. *Nat. Nanotechnol.* **2020**, *15* (2), 131−137.
(41) Wang, L.; Xu, X.; Zhang, L.; Qiao, R.; Wu, M.; Wang, Z.; Zhang, S.; Liang, J.; Zhang, Z.; Zhang, Z.; Chen, W.; Xie, X.; Zong, J.; Shan, Y.; Guo, Y.; Willinger, M.; Wu, H.; Li, Q.; Wang, W.; Gao, P.; Wu, S.; Zhang, Y.; Jiang, Y.; Yu, D.; Wang, E.; Bai, X.; Wang, Z. J.; Ding, F.; Liu, K. Epitaxial growth of a 100-square-centimetre single-crystal hexagonal boron nitride monolayer on copper. *Nature* **2019**, *570* (7759), 91−95.
(42) Tran, T. T.; Bray, K.; Ford, M. J.; Toth, M.; Aharonovich, I. Quantum emission from hexagonal boron nitride monolayers. *Nat. Nanotechnol.* **2016**, *11* (1), 37−41.
(43) Dean, C. R.; Wang, L.; Maher, P.; Forsythe, C.; Ghahari, F.; Gao, Y.; Katoch, J.; Ishigami, M.; Moon, P.; Koshino, M.; Taniguchi, T.; Watanabe, K.; Shepard, K. L.; Hone, J.; Kim, P. Hofstadter's butterfly and the fractal quantum Hall effect in moiré superlattices. *Nature* **2013**, *497* (7451), 598−602.
(44) Wang, E.; Lu, X.; Ding, S.; Yao, W.; Yan, M.; Wan, G.; Deng, K.; Wang, S.; Chen, G.; Ma, L.; Jung, J.; Fedorov, A. V.; Zhang, Y.; Zhang, G.; Zhou, S. Gaps induced by inversion symmetry breaking and second-generation Dirac cones in graphene/hexagonal boron nitride. *Nat. Phys.* **2016**, *12* (12), 1111−1115.
(45) Liang, J.; Song, Q.; Lin, J.; Li, G.; Fang, Y.; Guo, Z.; Huang, Y.; Lee, C. S.; Tang, C. In Situ Cu-Loaded Porous Boron Nitride Nanofiber as an Efficient Adsorbent for CO_2 Capture. *ACS Sustainable Chem. Eng.* **2020**, *8* (19), 7454−7462.
(46) Lee, S. Y.; Jung, H.; Kim, N. K.; Oh, H. S.; Min, B. K.; Hwang, Y. J. Mixed Copper States in Anodized Cu Electrocatalyst for Stable and Selective Ethylene Production from CO_2 Reduction. *J. Am. Chem. Soc.* **2018**, *140* (28), 8681−8689.

https://doi.org/10.1021/acs.nanolett.1c01258
Nano Lett. 2021, 21, 4469−4476

(47) Varela, A. S.; Kroschel, M.; Reier, T.; Strasser, P. Controlling the selectivity of CO_2 electroreduction on copper: The effect of the electrolyte concentration and the importance of the local pH. *Catal. Today* **2016**, *260*, 8−13.
(48) Nie, X.; Luo, W.; Janik, M. J.; Asthagiri, A. Reaction mechanisms of CO_2 electrochemical reduction on Cu(111) determined with density functional theory. *J. Catal.* **2014**, *312*, 108−122.

https://doi.org/10.1021/acs.nanolett.1c01258
Nano Lett. 2021, 21, 4469−4476